

Supporting information for: “Pressure-induced structural transition of mature HIV-1 Protease from a combined NMR/MD simulation approach”

Julien Roche¹, John M. Louis¹, Ad Bax¹ and Robert B. Best^{1*}

¹Laboratory of Chemical Physics, National Institute of Diabetes and Digestive and Kidney Diseases, National Institutes of Health, Bethesda, MD 20892 (USA).

Supporting Figures:

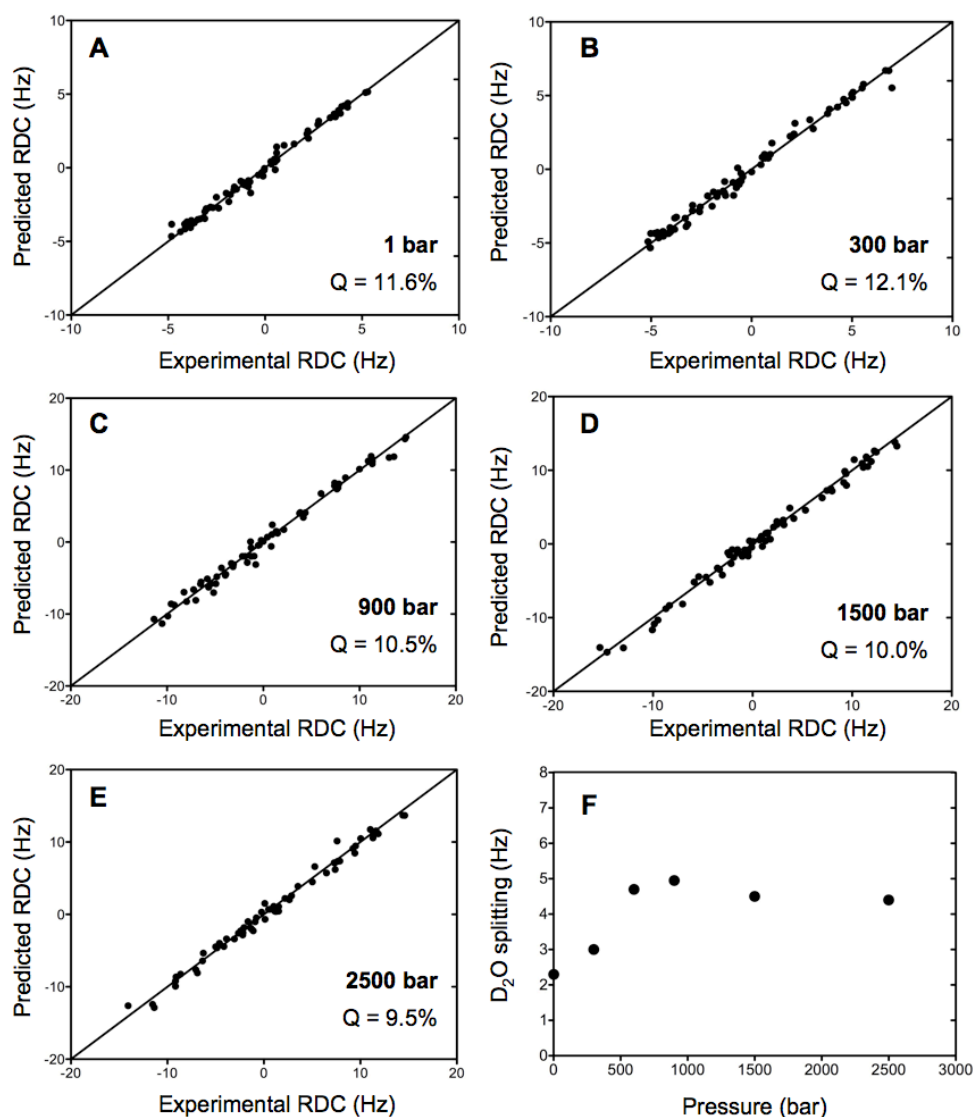


Figure S1: A-E: Comparison between the experimental $^1D_{NH}$ backbone RDCs measured at various pressures for a 0.6 mM sample of uniformly $^2H/^{13}C/^{15}N$ labeled ubiquitin with those predicted for the NMR refined structure 2MJB.¹ The alignment of the sample was obtained by using a paranematic dilute solution of Pf1 at 7 mg/ml and 200 mM NaCl. All data were recorded at 298 K. F: Quadrupolar splitting of HDO solvent signal measured for the aligned sample as a function of pressure.

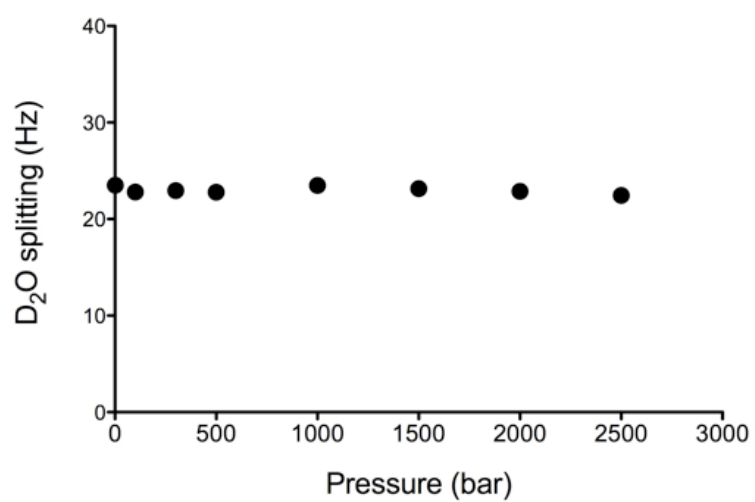


Figure S2: ²H quadrupolar splitting of D₂O measured for a liquid crystalline suspension of 10 mg/ml of squalamine at 293 K, from 1 bar to 2500 bar.

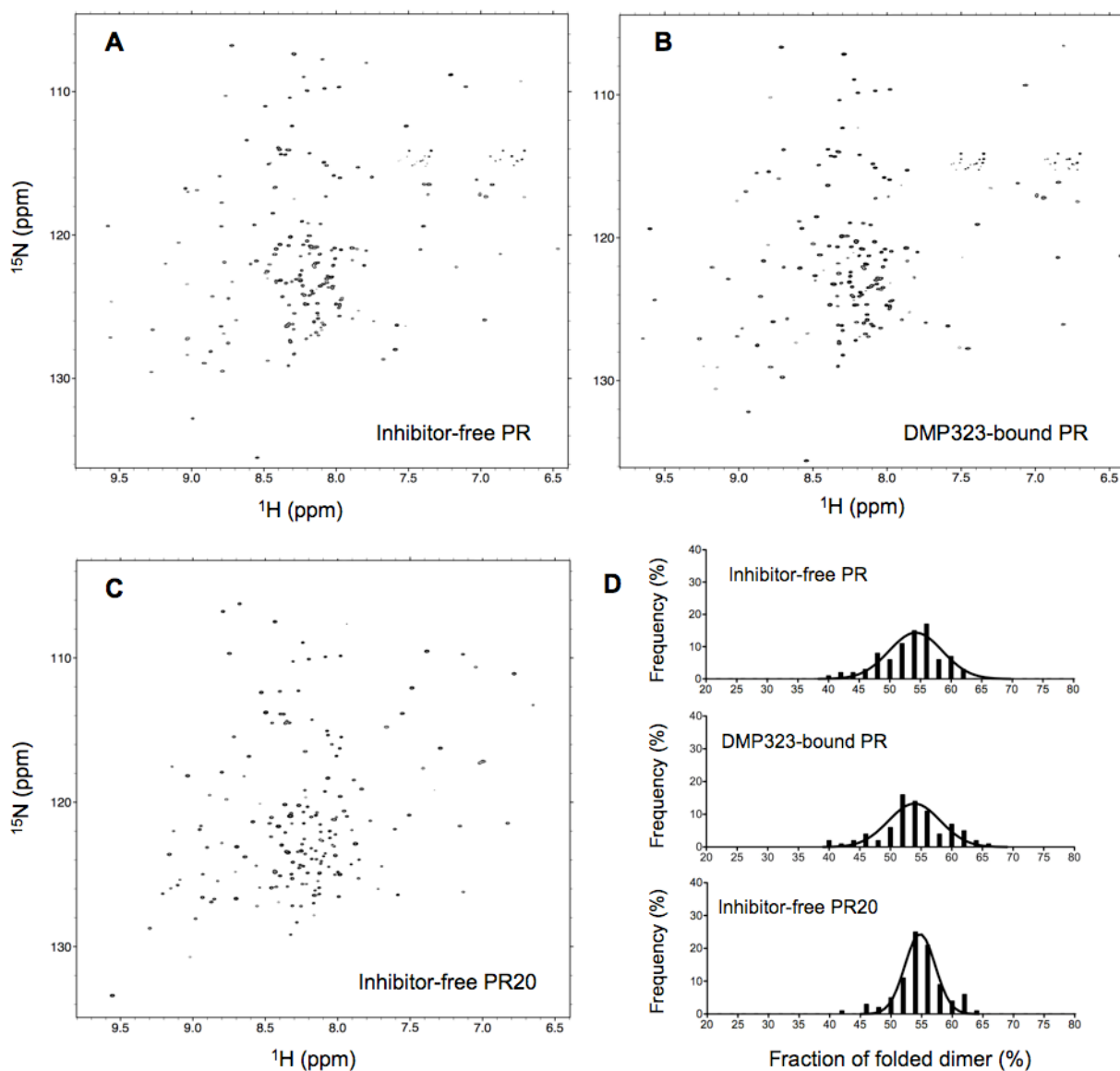


Figure S3: ^1H - ^{15}N TROSY-HSQC spectra of (A) the inhibitor-free PR (600 bar), (B) the DMP323-PR complex (500 bar) and (C) the inhibitor-free PR20 (600 bar), measured for the aligned samples in the dilute solution of squalamine. The pressure-induced unfolding being characterized by a slow-exchange process, the cross-peaks corresponding to both the folded and the unfolded states are visible. The assignment of the folded state in those conditions was determined by monitoring the evolution of the ^1H , ^{15}N chemical shifts from 1 bar to 200 bar and 400 bar. **D:** Distribution of the folded dimer population estimated for the three PR samples as the fraction of the individual amide cross peak intensity between 600 bar (or 500 bar for the DMP323-bound PR) and 1 bar.

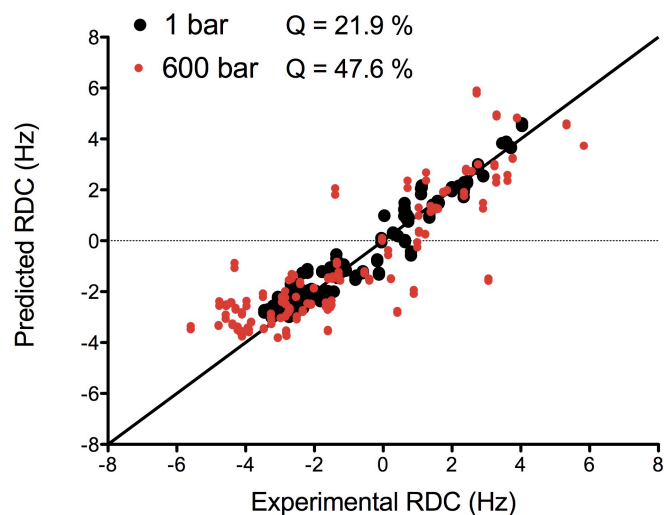


Figure S4: Correlation between the $^1\text{D}_{\text{NH}}$ RDCs measured for the inhibitor-free PR at 1 bar (black dots) and at 600 bar (red dots), and those predicted for the reference crystal structure, PDB entry 3BVB to which hydrogens were added with the program MOLMOL²

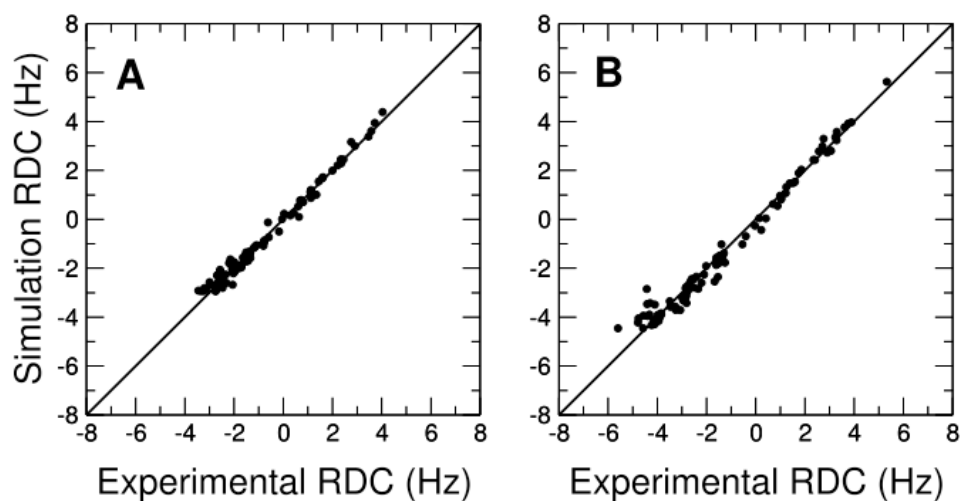


Figure S5. Agreement of RDC-biased simulations with the experimental data. Shown are the ensemble-averaged RDCs over the restrained simulations at (A) 1bar and (B) 600 bar.

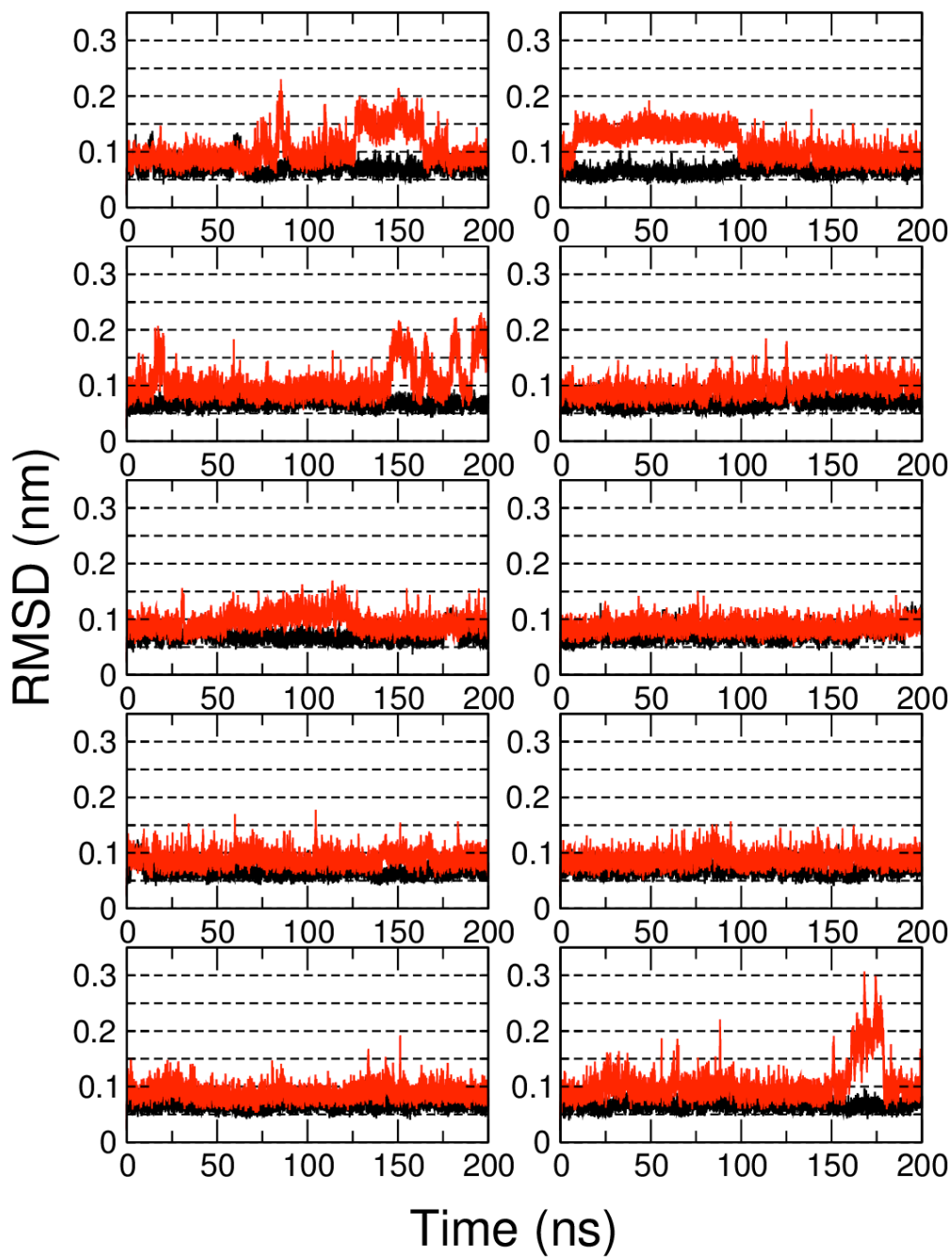


Figure S6. RMSD to reference structures in 1-bar simulations with AMBER ff99SBws force field, using 1-bar restraints. Black and red curves are the backbone heavy atom RMSD to the 3BVB structure, and to the “core” region (residues 10-23+62-73+87-93) and “flap” region (residues 30-61+74-84), respectively. The ten panels are replicates of the simulation with different initial velocities.

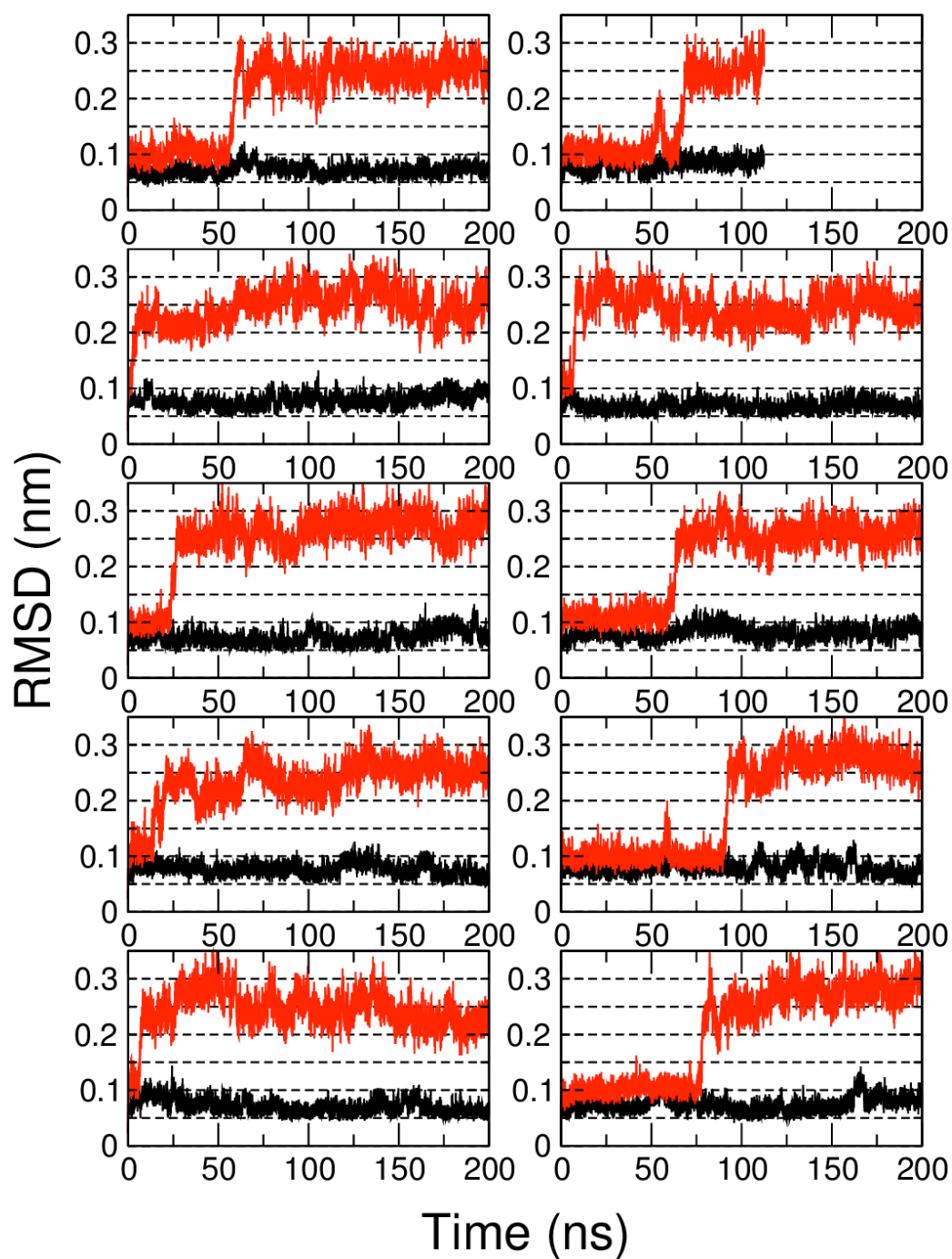


Figure S7. RMSD to reference structures in 600-bar simulations with AMBER ff99SBws force field, using 600 bar restraints. Black and red curves are the backbone heavy atom RMSD to the 3BVB structure, and to the “core” region (residues 10-23+62-73+87-93) and “flap” region (residues 30-61+74-84), respectively. The ten panels are replicates of the simulation with different initial velocities. The simulation in the second panel was terminated early.

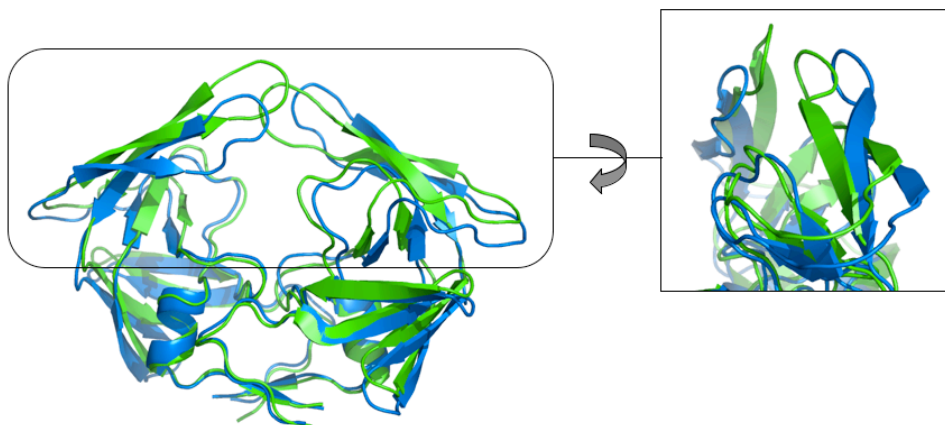


Figure S8. Comparison between the central structure of the “open” cluster obtained from the restrained MD simulations at 600 bar and the wide-open X-ray of the drug-resistant mutant PR20 (3UF3³)

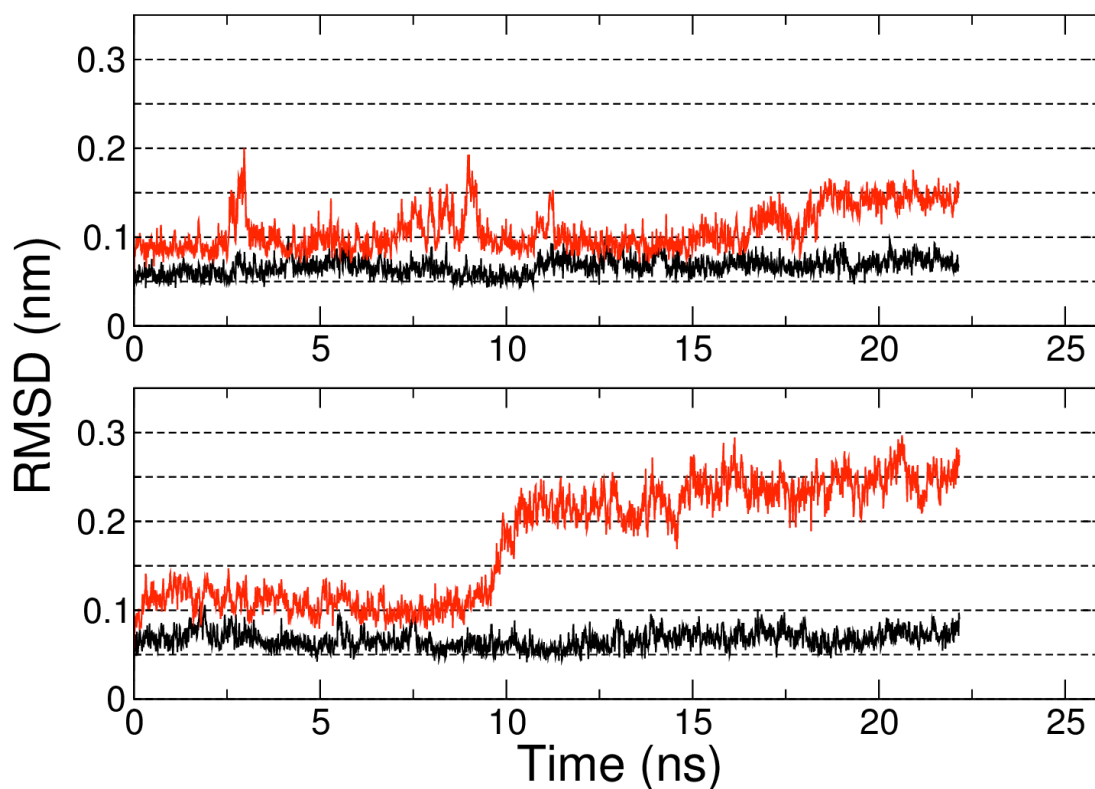


Figure S9. RMSD to reference structures in 600-bar simulations with CHARMM 36 force field, using 600 bar restraints. Black and red curves are the backbone heavy atom RMSD to the 3BVB structure, and to the “core” region (residues 10-23+62-73+87-93) and “flap” region (residues 30-61+74-84), respectively. The ten panels are replicates of the simulation with different initial velocities. The simulation in the second panel was terminated early.

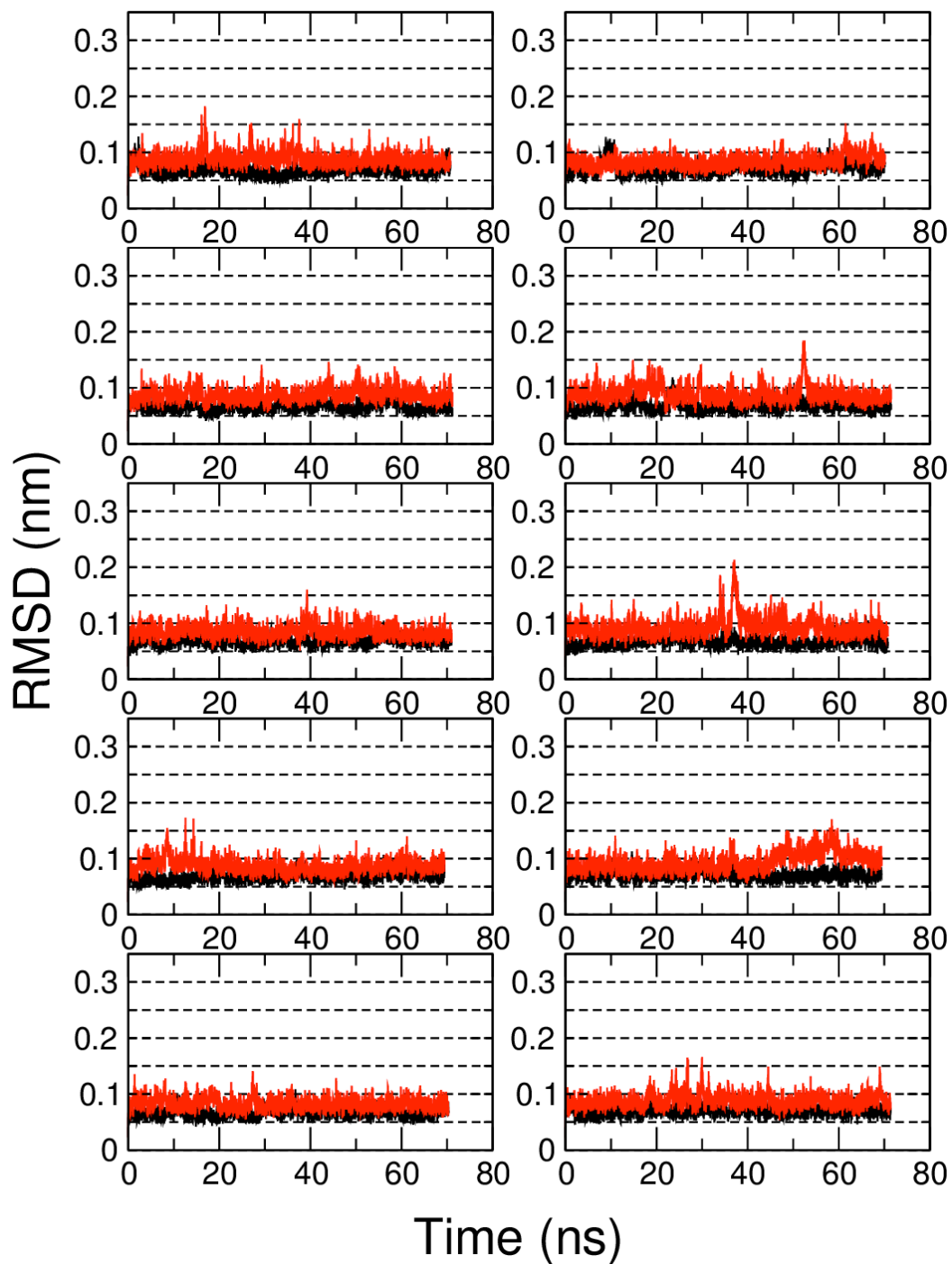


Figure S10. RMSD to reference structures using 1-bar restraints at a simulation pressure of 600 bar with AMBER ff99SBws force field. Black and red curves are the backbone heavy atom RMSD to the 3BVB structure, and to the “core” region (residues 10-23+62-73+87-93) and “flap” region (residues 30-61+74-84), respectively. The ten panels are replicates with different initial velocities.

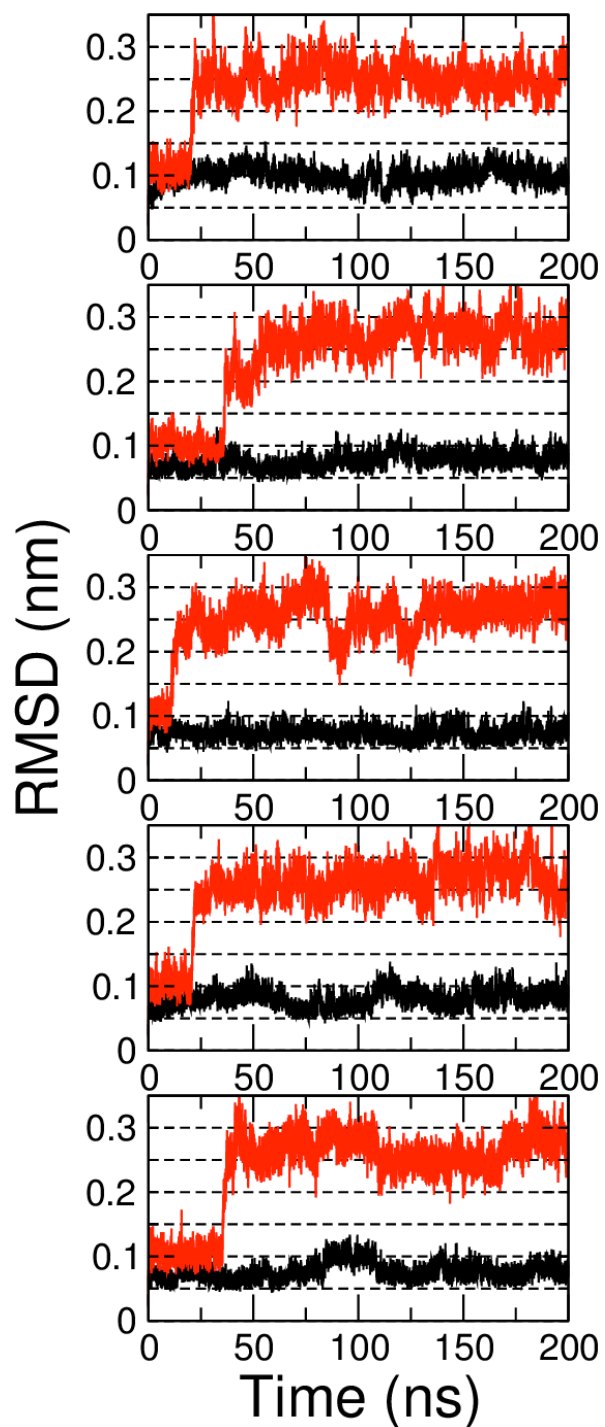


Figure S11. RMSD to reference structures using 600-bar RDC restraints at a simulation pressure of 1 bar using the AMBER ff99SBws force field. Black and red curves are the backbone heavy atom RMSD to the 3BVB structure, and to the “core” region (residues 10-23+62-73+87-93) and “flap” region (residues 30-61+74-84), respectively. The 5 panels are replicates with different initial velocities.

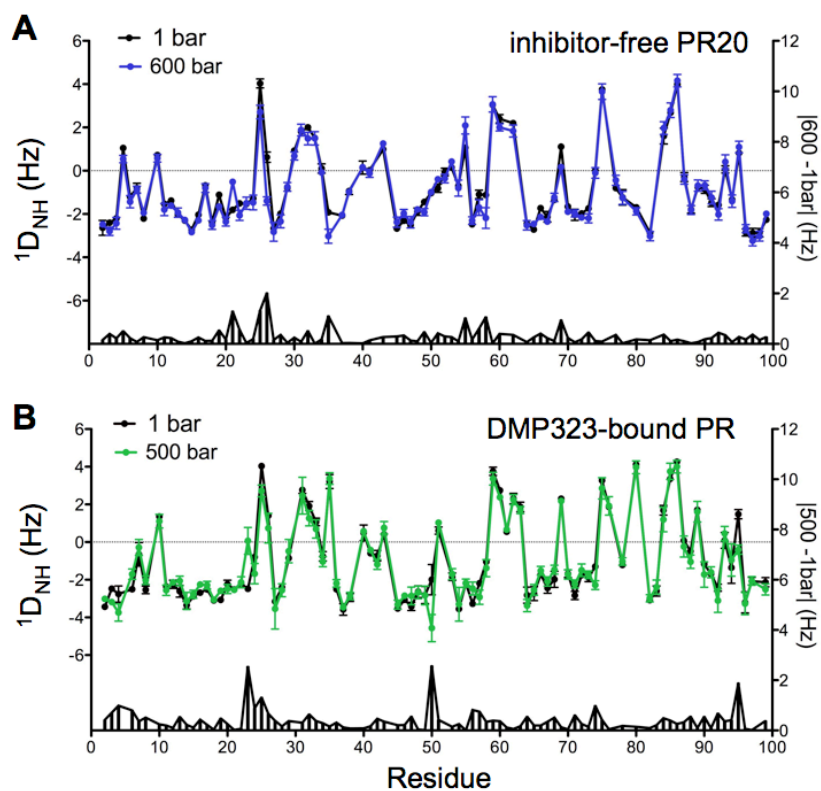


Figure S12. Backbone $^1D_{NH}$ RDCs measured for (A) the inhibitor-free PR20 and (B) the DMP-bound PR, under atmospheric (black) and high-pressure conditions (PR20 at 600 bar, blue; DMP-bound at 500 bar, green). The absolute difference between the atmospheric and high-pressure RDC data sets is shown on the right y-axis of the corresponding panel

Supporting Tables:

Table S1. $^1J_{\text{NH}}$ couplings and $^1D_{\text{NH}}$ RDCs measured for the inhibitor-free PR and the DMP323-bound PR at atmospheric and high-pressure conditions. The average experimental error is 0.05 Hz in the measured $^1J_{\text{NH}}$ and 0.15 Hz in the measured $^1D_{\text{NH}}$.

Residue	Inhibitor-free PR $^1J_{\text{NH}}$ (Hz)	Inhibitor-free	Inhibitor-free	DMP323-	DMP323-bound	DMP323-bound
		PR $^1D_{\text{NH}}$ (Hz) 1 bar	PR $^1D_{\text{NH}}$ (Hz) 600 bar	bound PR $^1J_{\text{NH}}$ (Hz)	PR $^1D_{\text{NH}}$ (Hz) bar	PR $^1D_{\text{NH}}$ (Hz) 500 bar
Q2	-91.9	-3.2	-3.8	-91.8	-3.4	-3.0
V3	-93.4	-2.5	-4.6	-93.1	-2.5	-3.2
T4	-92.7	-2.6	-3.9	-93.0	-2.8	-3.7
W6	-92.5	-1.2	-0.4	-92.4	-2.5	-1.7
Q7	-91.5	0.6	-0.1	-91.7	-0.7	-0.3
R8	-93.6	-2.6	-2.9	-93.4	-2.5	-2.0
L10	-92.1	0.7	1.4	-92.5	1.4	1.1
V11	-93.2	-2.0	-4.4	-93.0	-2.4	-2.6
T12	-92.4	-1.5	-2.5	-92.4	-2.2	-2.1
I13	-93.1	-2.5	-3.5	-92.9	-2.6	-2.1
K14	-92.0	-3.0	-4.4	-92.4	-3.4	-3.1
I15	-93.9	-2.3	-3.3	-93.7	-2.9	-2.8
G16	-94.8	-2.0	-4.0	-94.5	-2.7	-2.3
G17	-93.9	-2.1	-2.1	-93.2	-2.5	-2.3
Q18	-92.7	-3.2	-3.1	-92.1	-3.1	-3.1
L19	-92.3	-2.5	-3.3	-92.9	-3.1	-2.6
K20	-93.4	-1.7	-1.5	-93.2	-2.2	-2.5
E21	-92.1	-2.1	-2.7	-92.5	-2.5	-2.5
A22	-93.5	-1.6	-2.2	-93.4	-2.2	-2.1
L23	-91.7	-1.4	-1.3	-91.9	-2.5	0.1
L24				-94.5	-0.8	-1.7
N25	-94.6	4.0	2.7	-92.8	4.0	2.7
T26	-93.4	-0.6	-1.4	-92.0	1.4	0.7
G27	-92.1	-2.7	-2.8	-93.9	-3.2	-3.5
A28	-95.0	-2.0	-2.3	-93.7	-2.4	-2.6
D29	-93.1	-1.1	-1.6	-92.9	-0.9	-0.5
T31	-92.7	1.6	1.9	-92.8	2.8	2.5
V32	-91.0	1.4	2.4	-91.9	1.9	1.3
L33	-92.5	0.7	2.9	-93.1	1.1	0.7
E34	-92.9	-0.2	-1.3	-93.2	-0.8	-1.0
E35	-92.3	2.4	3.2	-92.6	3.2	3.4
M36	-92.3	-2.7	-1.6	-92.4	-2.5	-2.2
S37	-93.0	-2.8	-2.8	-93.1	-3.6	-3.5
L38	-92.7	-2.0	-2.8	-93.1	-2.9	-2.9
G40	-93.8	-0.1	1.0	-93.9	0.5	0.6
R41	-92.2	-1.5	-1.3	-92.0	-0.6	-0.4
W42	-92.7	0.4	1.2	-92.2	-0.7	-1.2
K43	-92.3	1.3	1.5	-92.7	0.4	0.8
K45	-93.3	-3.5	-4.2	-93.4	-3.5	-3.3
M46	-92.8	-3.1	-3.9	-92.8	-3.1	-2.8
I47	-93.2	-2.9	-3.5	-93.1	-3.4	-2.9
G48	-94.1	-2.7	-4.1	-94.0	-2.6	-2.7
G49				-94.1	-2.8	-2.8
I50	-92.4	-2.0	-4.6	-92.5	-2.0	-4.6
G51	-93.2	0.6	1.0	-93.1	0.6	1.0
G52	-93.9	-1.3	-2.0	-94.4	-1.8	-1.7
I54	-92.1	-2.1	0.4	-92.2	-3.6	-3.3
K55	-92.3	-2.3	-4.8	-92.4	-2.2	-2.2
V56	-93.7	-2.7	-4.1	-93.8	-3.3	-2.5
R57	-91.6	-1.5	-1.5	-91.6	-2.2	-2.9
Q58	-92.5	1.1	3.1	-92.4	-1.0	-1.4
Y59	-93.4	2.8	5.8	-93.0	3.8	3.4
D60	-92.8	2.9	3.8	-93.2	2.7	2.4
Q61	-92.4	1.1	0.7	-92.2	0.5	0.7
I62	-92.8	2.4	1.2	-92.9	2.3	2.2

L63	-92.6	2.0	3.3	-92.6	1.9	1.7
I64	-93.5	-2.5	-3.8	-93.7	-2.8	-3.4
E65	-92.3	-1.7	-2.8	-91.9	-2.7	-2.5
I66	-92.7	-2.2	-2.7	-92.8	-1.7	-1.5
L67	-93.7	-2.6	-4.3	-93.8	-2.4	-2.1
G68	-93.3	-1.5	-2.6	-93.3	-2.0	-1.5
H69	-92.1	1.6	1.7	-92.4	2.3	2.2
K70	-92.9	-1.5	-2.7	-92.7	-1.7	-1.7
A71	-93.3	-1.8	-3.0	-93.2	-2.8	-2.2
I72	-92.2	-1.6	-1.6	-92.7	-1.8	-1.5
G73	-95.9	-0.8	0.9	-95.4	-1.9	-1.7
T74	-92.0	-1.4	-4.3	-92.1	-1.3	-2.3
V75	-93.4	3.6	3.3	-93.4	3.3	2.9
L76	-92.5	2.2	2.6	-92.7	1.9	1.9
V77	-92.0	0.8	0.1			
G78	-94.1	-0.6	-1.5	-94.8	-1.2	-1.0
T80	-91.6	3.5	3.9	-91.5	4.1	4.0
V82	-91.4	-2.5	-2.5	-91.3	-3.1	-3.0
N83	-93.3	-2.6	-4.1	-93.1	-2.6	-2.4
I84	-92.7	1.1	2.4	-92.8	1.7	1.2
I85	-92.3	2.3	3.6	-92.2	3.4	3.8
G86	-94.1	3.7	5.3	-93.7	4.3	4.0
R87				-93.3	0.1	-0.2
N88	-95.5	-0.8	0.2	-95.1	-0.5	-1.0
L90	-93.6	-1.2	-0.5	-93.5	1.7	1.6
T91	-93.7	-1.4	-2.8	-93.4	-1.2	-1.7
Q92	-92.5	-2.2	-4.4	-92.6	-1.7	-1.6
I93	-92.1	0.3	1.0	-92.0	-2.4	-3.1
G94	-93.9	-0.8	-2.4	-93.7	0.1	0.5
A95	-93.8	0.1	1.6	-94.2	-1.4	-1.0
T96	-93.9	-2.5	-4.8	-93.8	1.5	-0.4
L97	-91.4	-2.1	-1.7	-91.2	-3.2	-3.3
N98	-92.6	-3.4	-5.6	-92.5	-2.1	-2.1
F99	-93.5	-2.7	-2.9	-93.4	-2.1	-2.5

Table S2. $^1J_{\text{NH}}$ couplings and $^1D_{\text{NH}}$ RDCs measured for the inhibitor-free PR20 at atmospheric and high-pressure conditions. The average experimental error is 0.05 Hz in the measured $^1J_{\text{NH}}$ and 0.15 Hz in the measured $^1D_{\text{NH}}$.

	Inhibitor-free PR20 $^1J_{\text{NH}}$ (Hz)	Inhibitor-free PR20 $^1D_{\text{NH}}$ (Hz) 1 bar	Inhibitor-free PR20 $^1D_{\text{NH}}$ (Hz) 600 bar
Q2	-91.7	-2.6	-2.5
I3	-93.0	-2.4	-2.8
T4	-93.2	-2.2	-2.4
L5	-93.1	1.1	0.5
W6	-92.6	-1.2	-1.4
K7	-91.4	-0.8	-0.9
R8	-93.2	-2.2	-1.9
F10	-92.0	0.7	0.6
V11	-93.2	-1.5	-1.8
T12	-92.5	-1.4	-1.6
V13	-93.5	-2.0	-1.9
K14	-92.1	-2.3	-2.3
I15	-94.0	-2.7	-2.8
G16	-94.7	-2.0	-2.3
G17	-93.5	-0.7	-0.8
Q18	-92.6	-2.4	-2.5
L19	-92.1	-1.1	-1.7
K20	-93.8	-2.2	-2.4
E21	-92.3	-1.8	-0.5
A22	-93.4	-1.5	-2.1
L23	-91.7	-1.5	-1.5
L24	-92.4	-1.3	-1.5
N25	-94.5	4.0	2.7
T26	-93.3	0.6	-1.4
G27	-92.2	-2.7	-2.8
A28	-94.7	-2.0	-2.3
D29	-93.0	-0.8	-0.7
N30	-92.4	0.9	0.7
T31	-93.1	1.8	1.9
I32	-91.1	2.0	1.5
F33	-92.4	1.5	1.5
E34	-92.7	0.1	-0.1
D35	-92.2	-1.9	-3.0
N37	-93.1	-2.1	-2.0
L38	-93.1	-0.9	-1.0
G40	-93.7	0.1	0.2
R41	-92.2	0.0	-0.1
K43	-92.4	1.0	1.3
K45	-93.2	-2.7	-2.4
M46	-92.6	-2.3	-2.0
V47	-92.9	-2.5	-2.4
G48	-94.0	-1.9	-1.8
G49	-93.6	-1.4	-1.9
I50	-92.3	-1.0	-1.0
G51	-93.5	-0.8	-0.4
G52	-93.8	-0.1	-0.4
F53	-93.1	0.2	0.4
L54	-92.4	-0.7	-0.8
K55	-92.3	-1.9	-0.8
V56	-93.6	-2.5	-2.3
R57	-91.2	-1.1	-1.7
E58	-92.3	-1.1	-2.2
Y59	-93.3	3.0	3.1
D60	-92.7	2.4	2.0
V62	-92.9	2.2	1.8
I64	-93.5	-2.4	-2.5
E65	-92.1	-2.7	-2.5
I66	-92.6	-1.7	-2.1
A67	-93.8	-2.1	-2.3
G68	-93.2	-1.3	-1.2
H69	-91.9	1.1	0.2

K70	-92.9	-1.7	-1.9
A71	-93.2	-2.0	-2.0
I72	-92.3	-2.0	-2.2
G73	-95.8	-1.7	-2.2
T74	-92.1	0.0	-0.1
V75	-93.4	3.8	3.7
V77	-92.4	-0.8	-0.4
G78	-94.2	-1.2	-1.3
T80	-91.6	-1.7	-1.9
V82	-91.3	-2.9	-3.0
V84	-92.9	1.6	2.0
I85	-92.1	2.7	2.8
G86	-94.2	4.0	4.2
R87	-93.2	-0.3	-0.4
D88	-95.4	-1.8	-1.8
T89	-94.0	-0.8	-0.7
M90	-93.9	-0.9	-0.7
T91	-93.8	-1.5	-1.2
Q92	-92.5	-1.6	-2.0
I93	-92.2	0.1	0.4
G94	-93.5	-1.3	-1.4
A95	-93.7	0.8	1.1
T96	-93.8	-2.9	-2.7
L97	-91.4	-2.9	-3.2
N98	-92.3	-2.9	-3.0
F99	-93.2	-2.3	-2.0

Table S3. Number of runs and total simulation length for each force field and set of conditions.

Force field / conditions	Number of runs	Total run time (ns)
Amber ff99SBw, 1 bar sim. press., 1 bar restraints	10	2000
Amber ff99SBw, 600 bar sim. press., 600 bar restraints	10	1912
Amber ff99SBw, 1 bar sim. press., 600 bar restraints	5	1000
Amber ff99SBw, 600 bar sim. press., 1 bar restraints	10	706
CHARMM36, 1 bar sim. press., 1 bar restraints	1	22
CHARMM36, 600 bar sim. press., 600 bar restraints	1	22

Table S4. Number of buried and surface waters. Errors are given in parentheses. We define three classes of water molecules: (i) bulk, those waters not in contact with any protein heavy atom; (ii) buried, those waters not in contact with any bulk waters and (iii) surface waters which comprise the remainder. Here, contacts between water molecules are defined as a distance between water oxygens of less than 3.5 Å, and contacts between water and proteins are defined as a water oxygen to protein heavy atom distance of less than 3.5 Å. Data are not shown for open conformations in conjunction with 1 bar restraints due to their negligible population with these restraints.

Simulation Pressure	Restraints from RDCs at pressure	Conformation	# buried waters	# surface waters
1 bar	1 bar	Closed	42.3 (0.3)	450.7 (0.5)
600 bar	600 bar	Closed	44.4 (0.5)	463.9 (0.8)
600 bar	600 bar	Open	45.4 (0.6)	474.1 (0.8)

References

1. Maltsev AS, Grishaev A, Roche J, Zasloff M, Bax A. Improved cross validation of a static ubiquitin structure derived from high precision residual dipolar couplings measured in a drug-based liquid crystalline phase. *J Am Chem Soc* 2014;136(10):3752-3755.
2. Koradi R, Billeter M, Wuthrich K. MOLMOL: a program for display and analysis of macromolecular structures. *J Mol Graph* 1996;14(1):51-55, 29-32.
3. Agniswamy J, Shen CH, Aniana A, Sayer JM, Louis JM, Weber IT. HIV-1 protease with 20 mutations exhibits extreme resistance to clinical inhibitors through coordinated structural rearrangements. *Biochemistry* 2012;51(13):2819-2828.